

Planar light bullets under conditions of second-harmonic generation

Sergey V. Sazonov*

*National Research Centre “Kurchatov Institute”,
1 Akademika Kurchatova Square, Moscow 123182, Russia*

Mikhail S. Mamaikin, Maria V. Komissarova, and Irina G. Zakharova

*Department of Photonics and Microwave Physics, Lomonosov Moscow State University,
1 Leninskie Gory Street, Moscow 119991, Russia*

(Received 3 February 2017; revised manuscript received 25 June 2017; published 16 August 2017)

We study solutions to second-harmonic-generation equations in two-dimensional media with anomalous dispersion. The analytical solution is obtained in an approximate form of the planar spatiotemporal two-component soliton by means of the averaged Lagrangian method. It is shown that a decrease in the amplitudes of both soliton components and an increase in the value of the transverse coordinate are accompanied by an increase in their temporal duration. Within this variational approach, we have managed to find a stability criterion for the light bullet and a period of oscillations of soliton parameters. Then, we use the obtained form as an initial configuration to carry out the direct numerical simulation of soliton dynamics. We demonstrate stable propagation of spatiotemporal solitons undergoing small oscillations predicted analytically for a long distance. The formation of a two-component light bullet is shown when we launch a pulse only at the fundamental frequency. In addition, we investigate the phase and group-velocity mismatch effects on the propagation of pulses.

DOI: [10.1103/PhysRevE.96.022208](https://doi.org/10.1103/PhysRevE.96.022208)**I. INTRODUCTION**

Solitons represent solitary waves with specific particlelike features, and they have been attracting a great deal of attention among scientists over the past few decades. One of the reasons for the interest in solitons has been the potential to create self-supporting fully localized waves known as spatiotemporal solitons, which freely propagate in a nonlinear medium. Such self-trapped two- and three-dimensional modes are a result of the competition between the nonlinear self-compression of the wave field and the linear effects of diffraction and dispersion aiming to stretch wave packets in spatial and temporal directions. Spatiotemporal optical solitons are often called “light bullets” in the literature. They may have either great theoretical significance or practical applications in the form of ultrafast all-optical data-processing schemes with switching rates of several terahertz [1], and highly precise interferometry by three-dimensional (3D) matter-wave solitons [2].

In contrast to normally stable 1D solitons, light bullets (being, in fact, 2D and 3D patterns) are highly unstable in a medium with Kerr (cubic) nonlinearity [3]. This self-attractive nonlinearity after finite propagation leads to the spontaneous formation of a singularity known as critical and supercritical collapse in 2D and 3D geometries, respectively. However, there are a variety of mechanisms that can prevent the destabilizing wave collapse, including nonlocal nonlinearity [4], saturation of nonlinearity [5], competing nonlinearities [6], higher-order diffraction or dispersion [7], or dispersive coupling [8].

It is well known that the occurrence of a collapse depends on both the dimension of a soliton and the power of the nonlinearity. As demonstrated in [3,9], wave collapse in a second-harmonic-generation system does not take place in all

dimensions, including the transverse coordinates and time. Therefore, the self-focusing collapse is precluded in a bulk quadratic nonlinear crystal. This fact allows us to get stable light bullets in such media, which have a lower excitation threshold in comparison with a cubic one. The two-component structure at the fundamental and second frequencies is a distinctive feature of quadratic solitons. The coupled state is formed from both waves without energy exchange, and two harmonics propagate as one solitary wave.

In the past two decades, experimental observations of light bullets in quadratic media have been reported by numerous authors; see, for example, [10,11]. In particular, it was recently demonstrated that competing cascaded-quadratic and intrinsic cubic nonlinear responses may be used for the control of filamentation and second-harmonic-generation dynamics in birefringent nonlinear media [12].

Considering this problem, one should note that theoretical results have been obtained mainly using numerical simulation [13–15]. Some examples of analytical results include the construction in an analytical form of a full family of approximate stationary (z -independent) soliton solutions to second-harmonic-generation equations with group-velocity matching [16], and the analysis of dispersive modulational instability of spatial solitons due to nondegenerate three-wave mixing [17].

In the present work, we analyze the possibility of the formation and stable propagation of light bullets in quadratic nonlinear media with anomalous dispersion for both harmonics. Unlike [16], we generalize the consideration of the problem, and we derive a dynamic (z -dependent) solution. Provided that the phase- and group-matching conditions hold, the averaged Lagrangian method allows us to obtain an analytical solution in the form of a spatiotemporal soliton. In addition, we derive a stability condition and a period of small oscillations of light bullet parameters. The numerical simulation shows the robust propagation of the solitary wave with the period of

*sazonov.sergey@gmail.com

intensity oscillations predicted theoretically. In addition, we demonstrate the dynamics of the derived soliton when the phase- and group-velocity-matching conditions are absent.

The paper is organized as follows. In Sec. II we describe the system of basic equations, and we apply the averaged Lagrangian method to it. This application gives us a soliton solution in the form of a light bullet at both fundamental and second frequencies. Analytical analysis of stability is given in Sec. III. We present the results of direct numerical simulations, and we demonstrate a robust propagation of the derived solution in Sec. IV. Then, we demonstrate two-component soliton formation launching only the fundamental pulse at the input into the medium, and we discuss the physical situation in which the phase- and group-velocity-matching conditions are not complied with. In Sec. V we present the conclusions.

II. AVERAGED LAGRANGIAN METHOD

The system of second-harmonic generation for the envelopes of the fundamental a_1 and second a_2 harmonics, taking into account the mutual influence of nonlinearity, second-order diffraction, and dispersion, is written as [9,18]

$$i\left(\frac{\partial a_1}{\partial z} + \delta \frac{\partial a_1}{\partial \tau}\right) + \frac{\beta_2^{(1)}}{2} \frac{\partial^2 a_1}{\partial \tau^2} - \frac{c}{2n_1\omega} \Delta_{\perp} a_1 = \gamma_1 a_1^* a_2 \exp(-i\Delta k z), \quad (1)$$

$$i\left(\frac{\partial a_2}{\partial z} - \delta \frac{\partial a_2}{\partial \tau}\right) + \frac{\beta_2^{(2)}}{2} \frac{\partial^2 a_2}{\partial \tau^2} - \frac{c}{4n_2\omega} \Delta_{\perp} a_2 = \gamma_2 a_1^2 \exp(i\Delta k z), \quad (2)$$

where $\beta_2^{(1)}$ and $\beta_2^{(2)}$ are the coefficients of the group-velocity dispersion (GVD) at the fundamental and second harmonics, respectively, n_1 and n_2 are the refractive indexes of the fundamental and second harmonics, respectively, γ_1 and γ_2 are the quadratic nonlinearity coefficients proportional to the second-order nonlinear susceptibility $\chi^{(2)}$ for both harmonics, $\Delta k = 2\omega(n_1 - n_2)/c$ is the phase mismatch, c is the speed of light in vacuum, ω is the carrier frequency of fundamental harmonics, and δ is the mismatch of group velocities,

$$\tau = t - \frac{1}{2} \left(\frac{1}{v_{g1}} + \frac{1}{v_{g2}} \right) z, \quad \delta = \frac{1}{2} \left(\frac{1}{v_{g1}} - \frac{1}{v_{g2}} \right).$$

In our analysis, we consider planar diffraction ($\Delta_{\perp} = \partial^2/\partial x^2$) and suppose the phase- ($\Delta k = 0$, $n_1 = n_2 = n$) and group-velocity-matching ($\delta = 0$, $v_{g1} = v_{g2} = v_g$) conditions are fulfilled as well as the relation for GVD coefficients,

$$\beta_2^{(2)} = 2\beta_2^{(1)}. \quad (3)$$

Simultaneous fulfillment of these conditions will be discussed below.

Using the transformation $a_1 = \sqrt{\gamma_1/2\gamma_2} A_1$, $a_2 = A_2$, and then denoting $\beta_2 = \beta_2^{(1)}$ and $\gamma = \gamma_1$, we derive (1) and (2) in the following form:

$$i \frac{\partial A_1}{\partial z} - \frac{c}{2n\omega} \frac{\partial^2 A_1}{\partial x^2} + \frac{\beta_2}{2} \frac{\partial^2 A_1}{\partial \tau^2} - \gamma A_1^* A_2 = 0, \quad (4)$$

$$i \frac{\partial A_2}{\partial z} - \frac{c}{4n\omega} \frac{\partial^2 A_2}{\partial x^2} + \beta_2 \frac{\partial^2 A_2}{\partial \tau^2} - \frac{\gamma}{2} A_1^2 = 0. \quad (5)$$

To obtain a solution of the system (4) and (5), we apply the averaged Lagrangian method [19]. This is a well-known method, which was recently applied, for example, to the investigation of axially symmetric quadratic spatiotemporal solitons [20] and the solitonlike modes of generation of the highest harmonics [21].

Within this approach, we first find an exact 1D soliton solution for the equations under consideration in the paraxial approximation. Next, to proceed to transverse spatial effects, an assumption is made that some of the parameters in this solution depend on spatial coordinates. We refer to this solution as a trial one. It is substituted into the Lagrangian that corresponds to the initial system of equations involving derivatives with respect to transverse coordinates. Then the resulting expression is averaged over time. Finally, the averaged Lagrangian involving dependence on the variable parameters is obtained and applied to the Euler-Lagrange equations for these parameters.

As GVD coefficients are connected by the relation (3), the system (4) and (5) has the temporal ($\partial^2/\partial x^2 = 0$) soliton solution of the form [22]

$$A_1 = \pm \frac{6\beta_2}{4\tau_p^2\gamma} \exp\left(i \frac{\beta_2 z}{2\tau_p^2}\right) \operatorname{sech}^2\left(\frac{\tau}{2\tau_p}\right), \quad (6)$$

$$A_2 = -\frac{3\beta_2}{4\tau_p^2\gamma} \exp\left(i \frac{\beta_2 z}{\tau_p^2}\right) \operatorname{sech}^2\left(\frac{\tau}{2\tau_p}\right), \quad (7)$$

where τ_p is the duration of the pulses of both harmonics.

Now we consider transverse dynamics determined by the second terms in (4) and (5). The system (4) and (5) has the Lagrangian

$$L = L_1 + L_2 + L_{\text{int}}, \quad (8)$$

where

$$L_1 = \frac{i}{2} \left(A_1^* \frac{\partial A_1}{\partial z} - A_1 \frac{\partial A_1^*}{\partial z} \right) + \frac{c}{2n\omega} \left| \frac{\partial A_1}{\partial x} \right|^2 - \frac{\beta_2}{2} \left| \frac{\partial A_1}{\partial \tau} \right|^2, \quad (9)$$

$$L_2 = \frac{i}{2} \left(A_2^* \frac{\partial A_2}{\partial z} - A_2 \frac{\partial A_2^*}{\partial z} \right) + \frac{c}{4n\omega} \left| \frac{\partial A_2}{\partial x} \right|^2 - \beta_2 \left| \frac{\partial A_2}{\partial \tau} \right|^2, \quad (10)$$

$$L_{\text{int}} = -\frac{\gamma}{2} (A_1^{*2} A_2 + A_1^2 A_2^*). \quad (11)$$

In Ref. [16], trial solutions for A_1 and A_2 are chosen in the form of Gaussian profiles with respect to τ and transverse coordinates. Here we follow Refs. [23,24], i.e., the trial solutions are chosen similar to the temporal solitons (6) and (7),

$$A_1 = \pm \frac{6\beta_2}{\gamma} \mu^2 \exp(i\Phi_1) \operatorname{sech}^2(\mu\tau), \quad (12)$$

$$A_2 = -\frac{3\beta_2}{\gamma} \mu^2 \exp(i\Phi_2) \operatorname{sech}^2(\mu\tau), \quad (13)$$

where μ and $\Phi_1 = \Phi_2/2 = Q$ are the functions to be defined. Substituting (12) and (13) into (8)–(11) and integrating over

τ , we have

$$\int_{-\infty}^{+\infty} L d\tau = 216 \left(\frac{\beta_2}{\gamma} \right)^2 \Lambda, \quad (14)$$

where the averaged Lagrangian is

$$\Lambda = \frac{\mu^3}{3} \left[\frac{c}{2n\omega} \left(\frac{\partial Q}{\partial x} \right)^2 - \frac{\partial Q}{\partial z} \right] + \frac{2}{5} \beta_2 \mu^5 + \frac{c}{4n\omega} \left(1 + \frac{\pi^2}{30} \right) \mu \left(\frac{\partial \mu}{\partial x} \right)^2. \quad (15)$$

Using (15), we write down a system of Euler-Lagrange equations for μ and Q ,

$$\frac{\partial \rho}{\partial z} + \frac{\partial}{\partial x} \left(\rho \frac{\partial \phi}{\partial x} \right) = 0, \quad (16)$$

$$\frac{\partial \phi}{\partial z} + \frac{1}{2} \left(\frac{\partial \phi}{\partial x} \right)^2 + \frac{2c}{n\omega} \beta_2 \rho^{2/3} = \frac{2g^2}{\sqrt{\rho}} \frac{\partial^2 \sqrt{\rho}}{\partial x^2}, \quad (17)$$

where

$$g^2 = \frac{1}{6} \left(1 + \frac{\pi^2}{30} \right) \left(\frac{c}{n\omega} \right)^2, \quad \rho = \mu^3, \quad \phi = -\frac{c}{n\omega} Q. \quad (18)$$

In the 1D case ($\partial/\partial x = 0$), we find $\mu = 1/2\tau_p = \text{const}$ and $Q = \beta_2 z / (2\tau_p^2)$, which coincides with the parameters of the exact one-dimensional solution [see Eqs. (6) and (7) and Eqs. (12) and (13)]. The latter is an important argument in favor of the correctness of the averaged Lagrangian method. Note also that in the 1D case there are no oscillations of solitonic parameters. This result coincides with the conclusion of Ref. [25], where the variational approach for 1D solitons of the nonlinear Schrödinger equation was used.

If $g = 0$, the system (16) and (17) formally describes a nonstationary one-dimensional current of the ideal liquid, where the role of time is played by the z coordinate. The first equation is the continuity equation; the second equation is Cauchy's integral. It is worth noting that the case of $g = 0$ corresponds to the approximation of "geometrical optics". In turn, the right-hand side of (17) includes the effects of solitonic diffraction [21]. In this case, the set of equations (16) and (17) is similar to the equations describing the nonideal quantum Bose gas.

It is easy to see that the system (16) and (17) is equivalent to the equation for a complex function ψ ,

$$i \frac{\partial \psi}{\partial z} = -\frac{c\beta_2}{gn\omega} |\psi|^{4/3} \psi + g \frac{\partial^2 \psi}{\partial x^2}, \quad (19)$$

where

$$\psi = \sqrt{\rho} \exp \left(-i \frac{\phi}{2g} \right). \quad (20)$$

Equation (19) formally describes the propagation of a beam in a nonlinear planar medium. It is possible to name this equation "the modified nonlinear Schrödinger (or Gross-Pitaevskii) equation".

We seek a solution of Eq. (19) in the form

$$\psi = F(x) \exp(-ikz), \quad (21)$$

where κ is a constant. Substituting (21) into (19), we get

$$\frac{\partial^2 F}{\partial x^2} = \left(\frac{3}{4R_0} \right)^2 F - b F^{7/3}, \quad (22)$$

where

$$\frac{1}{R_0} = \frac{4}{3} \sqrt{\frac{\kappa}{g}}, \quad b = -\frac{c}{n\omega} \frac{\beta_2}{g^2}. \quad (23)$$

Analyzing (22) and (23), we conclude that (22) has a solution localized in the transversal directions under the condition $b > 0$, i.e., at $\beta_2 < 0$. Then R_0 represents the transversal width of the pulse. This solution looks like

$$F \equiv \sqrt{\rho} = \left(\frac{15}{16|\beta_2|} \frac{n\omega}{c} \frac{g^2}{R_0^2} \right)^{3/4} \text{sech}^{3/2} \left(\frac{x}{2R_0} \right). \quad (24)$$

Expressions (12), (13), (18), (20), (23), and (24) allow us to find the solution of the system (4) and (5) in the following explicit form:

$$A_1 = \pm A_0 \exp(iQ) \text{sech}^2 \left(\frac{x}{2R_0} \right) \text{sech}^2 \left(\frac{\tau}{2\tau_p} \right), \quad (25)$$

$$A_2 = \frac{A_0}{2} \exp(2iQ) \text{sech}^2 \left(\frac{x}{2R_0} \right) \text{sech}^2 \left(\frac{\tau}{2\tau_p} \right), \quad (26)$$

where

$$A_0 = \frac{15}{16} \left(1 + \frac{\pi^2}{30} \right) \frac{c}{n\omega\gamma R_0^2}, \quad (27)$$

$$Q = -\frac{3}{16} \frac{c}{n\omega} \left(1 + \frac{\pi^2}{30} \right) \frac{z}{R_0^2}, \quad (28)$$

$$\mu = \frac{1}{2\tau_p} = \frac{1}{2\tau_0} \text{sech} \left(\frac{x}{2R_0} \right). \quad (29)$$

Here the temporal duration τ_0 (or temporal width) of the soliton in the center (at $x = 0$) is related to its spatial width R_0 ,

$$R_0 = \sqrt{\frac{5(1 + \pi^2/30)}{8} \frac{c}{n\omega|\beta_2|}} \tau_0 = 0.91 \sqrt{\frac{c}{n\omega|\beta_2|}} \tau_0. \quad (30)$$

Let us determine the dispersion length l_{dis} and diffraction length l_D as

$$l_{\text{dis}} = \frac{2\tau_0^2}{|\beta_2|}, \quad l_D = \frac{n\omega}{c} R_0^2. \quad (31)$$

Then the expression (30) can be written in the form

$$l_D = \frac{5}{16} \left(1 + \frac{\pi^2}{30} \right) l_{\text{dis}} \approx 0.42 l_{\text{dis}}. \quad (30')$$

Thus, with a decrease of the temporal duration of the soliton, its transversal size becomes smaller while the amplitude increases.

At the choice of solutions in the form of Gaussian profiles, all parameters (amplitude, width, e.g.) are considered as constants [16]. In our approach, we do not postulate a type of profile, but we obtain it solving the corresponding equations. In the same way, we have found that the pulse duration depends on the transversal coordinate [see Eq. (29)].

III. STABILITY

Actually, the solution (25)–(30) corresponds to plane-wave fronts when the transversal width, temporal duration, and amplitude are constants. To investigate the stability of the stationary solution (25)–(30), we return to the set of equations (16) and (17).

The exact self-similar solution of Eq. (16) is as follows:

$$\rho = \rho_0 \frac{R_0}{R} G\left(\frac{x}{R}\right), \quad \phi = f + \frac{x^2}{2R} \frac{dR}{dz}, \quad (32)$$

where ρ_0 is a constant, R and f are unknown functions of z , and G is an unknown dimensionless function of x/R . Here we note that the second term in the expression for ϕ describes the dynamic curvature of wavefronts. In the solution (25)–(30), this curvature is absent and $R = R_0 = \text{const}$. Therefore, we may say that the solution (32) corresponds to some deviation from the steady-state solution (25)–(30) when the width of a soliton depends on the z coordinate. This dependence, in turn, causes a curvature of wavefronts.

The function R can be defined after substitution of (32) into (17). According to (24) and (18), we put approximately

$$G = \text{sech}^3\left(\frac{x}{2R}\right). \quad (33)$$

Substituting (32) and (33) into (17), we obtain

$$\begin{aligned} \frac{df}{dz} + \frac{x^2}{2R} \frac{d^2R}{dz^2} - \frac{2c|\beta_2|}{n\omega} \rho_0^{2/3} \frac{R_0^{2/3}}{R^{2/3}} \text{sech}^2\left(\frac{x}{2R}\right) \\ = \frac{9g^2}{8R^2} \left[1 - \frac{5}{3} \text{sech}^2\left(\frac{x}{2R}\right)\right]. \end{aligned} \quad (34)$$

Using the near-axis approximation [20,26]

$$(x/R)^2 \ll 1, \quad (35)$$

we have $\text{sech}^2(\xi) \approx 1 - \xi^2$. Then, equating the coefficients at x^0 and x^2 in the left-hand part with those in the right-hand part of (34), we get

$$\frac{df}{dz} = \frac{c|\beta_2|}{2n\omega\tau_0^2} \frac{R_0^{2/3}}{R^{2/3}} - \frac{3g^2}{4R^2}, \quad (36)$$

$$\frac{d^2R}{dz^2} = -\frac{c|\beta_2|}{4n\omega\tau_0^2} \frac{R_0^{2/3}}{R^{5/3}} + \frac{15g^2}{16R^3} = -\frac{dU}{dR}. \quad (37)$$

Here we assume that $\rho_0^{2/3} = 1/4\tau_0^2$ [see (18) and (28)]. Note that $n(df/dz)$ is a nonlinear addition to the refractive index.

Equation (37) is formally similar to an equation of motion of a material point of the unit mass in the field with the potential energy (see Fig. 1)

$$U = -\frac{3c|\beta_2|}{8n\omega\tau_0^2} \frac{R_0^{2/3}}{R^{2/3}} + \frac{15g^2}{32R^2}. \quad (38)$$

Let us assume in (37) that $dU/dR = 0$. Then we find that $R = R_0 = \text{const}$ [see Eq. (30)]. Substituting (30) into (36) and taking into account (32) and (18), we obtain the expression (28). Thus, the solution (25)–(30) is stable with respect to small perturbations happening near the minimum of function $U(R)$ (see Fig. 1). If perturbations are not small, then the general analysis on the basis of Eqs. (37) and (38) does not



FIG. 1. Potential energy vs R .

create a difficulty. For example, let the initial wavefronts be flat, i.e., $(dR/dz)|_{z=0} = 0$.

It is apparent that, if $U > 0$, there is an irreversible spatiotemporal broadening of the pulse. Therefore, to find a stability condition, we assume that $U < 0$ and $R = R_{\text{in}} \neq R_0$. Then we obtain

$$R_{\text{in}}^{4/3} > \frac{5n\omega}{4c} g^2 \frac{\tau_0^2}{|\beta_2|R_0^{2/3}},$$

where R_{in} is the transversal width corresponding to an input state of the light bullet. This inequality and (30) result in

$$R_{\text{in}} > R_m \equiv \left(\frac{1}{3}\right)^{3/4} R_0 = 0.44 R_0. \quad (39)$$

Here R_m is the transversal width at zero potential energy.

Defining the input diffraction length as $l_D^{\text{in}} = (n\omega/c)R_{\text{in}}^2$, we rewrite the condition (39), taking into account (30), as follows:

$$l_D^{\text{in}} > \frac{5}{48\sqrt{3}} \left(1 + \frac{\pi^2}{30}\right) l_{\text{dis}} = 0.08 l_{\text{dis}}. \quad (39a)$$

We highlight that the condition (39a) is valid if wavefronts of an input pulse are flat.

Let us define a spatial period of small oscillations of the parameters of the light bullet, assuming in (37) $R = R_0 + \zeta$. After the linearization of Eq. (37) with respect to ζ , we have

$$\frac{d^2\zeta}{dz^2} + \Omega_s^2 \zeta = 0,$$

where $\Omega_s^2 = 2/(3l_{\text{dis}}l_D)$. This equation gives us the expression for the spatial period of oscillations $T_s = 2\pi/\Omega_s$,

$$T_s = \pi\sqrt{6l_{\text{dis}}l_D}.$$

Taking into account (30)', we rewrite this expression as

$$T_s = 4.96 l_{\text{dis}} = 11.94 l_D. \quad (40)$$

Oscillations of the transversal width of the bullet are accompanied by oscillations of the amplitude, temporal duration, phase velocity, and the curvatures of phase wavefronts. If the equality (30) [see also (30)'] holds at the input into the medium, then the oscillations of the solitonic parameters are rather insignificant.

To analyze the stability of the obtained solutions, we have used the approach described in this section. At the same time, we did not apply the Vakhitov-Kolokolov stability criterion. We believe that our approach supplements the methods used in Ref. [16].

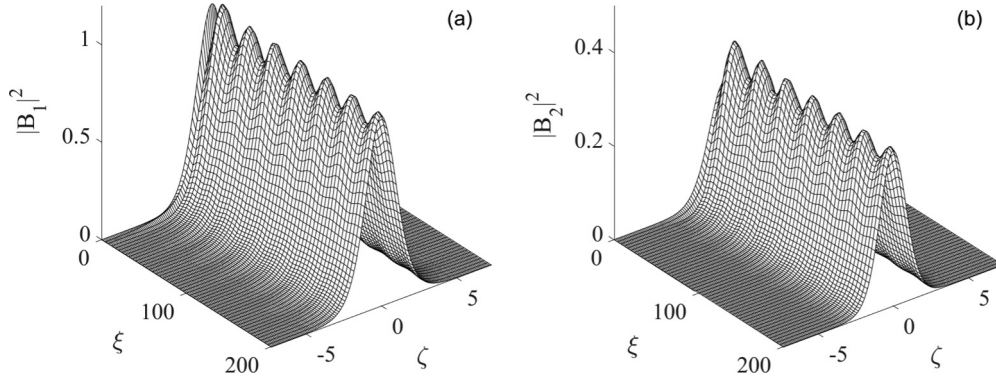


FIG. 2. Dynamics of spatial intensity profiles of (a) fundamental and (b) second harmonics vs the propagation distance.

IV. NUMERICAL SIMULATION

In this section, we study the dynamics of the system (4) and (5) and the system (1) and (2) by means of numerical modeling. It is worth noting that the system (1) and (2) possesses the following integrals of motion, which we present in dimensionless form:

$$E(\xi) = \iint (|B_1|^2 + 2|B_2|^2) d\zeta d\eta, \quad (41)$$

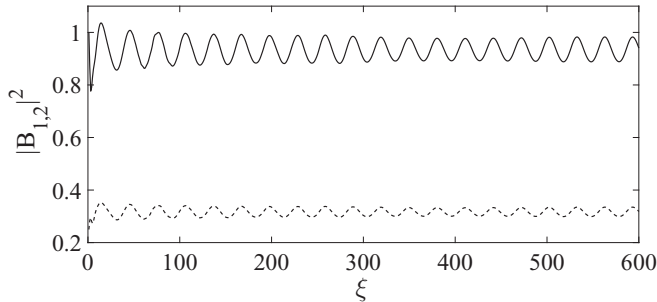


FIG. 3. Peak intensities of the fundamental (solid line) and second (dashed line) harmonics vs the propagation distance when inputting the derived solution (25)–(29).

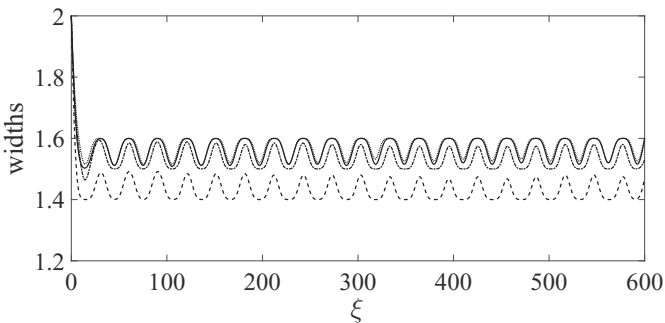


FIG. 4. Spatial and temporal widths of the fundamental (solid and dashed-dotted lines, respectively) and second (dashed and dotted lines, respectively) harmonics vs the propagation distance when inputting the derived solution (25)–(29).

$$H(\xi) = \iint \left[l_\eta \left(\left| \frac{\partial B_1}{\partial \eta} \right|^2 + 2 \left| \frac{\partial B_2}{\partial \eta} \right|^2 \right) + \sigma |B_1|^2 \frac{\partial \Phi_1}{\partial \eta} - \sigma |B_2|^2 \frac{\partial \Phi_2}{\partial \eta} - \frac{1}{4} l_\zeta \left(2 \left| \frac{\partial B_1}{\partial \zeta} \right|^2 + \left| \frac{\partial B_2}{\partial \zeta} \right|^2 \right) + \text{Re} [B_1^2 B_2^* \exp(i \Delta q \xi)] \right] d\zeta d\eta. \quad (42)$$

The integrals (41) and (42) are normalized in the following way: $B_1 = A_1/A_{\text{in}}$, $B_2 = A_2/A_{\text{in}}$, $\xi = z/l_{\text{nl}}$, $\zeta = x/R_{\text{in}}$, $\eta = \tau/\tau_{\text{in}}$, $\sigma = (\delta/\tau_{\text{in}})l_{\text{nl}}$, $\Delta q = \Delta k l_{\text{nl}}$, $l_\zeta = l_{\text{nl}}/l_{\text{D}}^{\text{in}}$, and $l_\eta = l_{\text{nl}}/l_{\text{dis}}^{\text{in}}$, where A_{in} is the input peak amplitude of the fundamental harmonic, τ_{in} is the initial time duration, and $l_{\text{nl}} = 1/\gamma A_{\text{in}}$ is the nonlinear length. Let us recall that the phases of harmonics are defined in the standard way, $B_j = |B_j| \exp(i \Phi_j)$, $j = 1, 2$ [see also (12) and (13)].

Our computations were carried out on the basis of a symmetrical nonlinear difference scheme from the well-known class of spectral methods [27,28]. We chose the following computational parameters: the range of step size along the propagation coordinate was $\Delta \xi = 0.1\text{--}0.5$, while the range of step size along space and time coordinates was $\Delta \zeta = 0.05\text{--}0.1$, $\Delta \eta = 0.05\text{--}0.1$. Typical lattice sizes in our simulations were 2048×2048 points in the spatial and temporal dimensions, respectively. The transversal integration

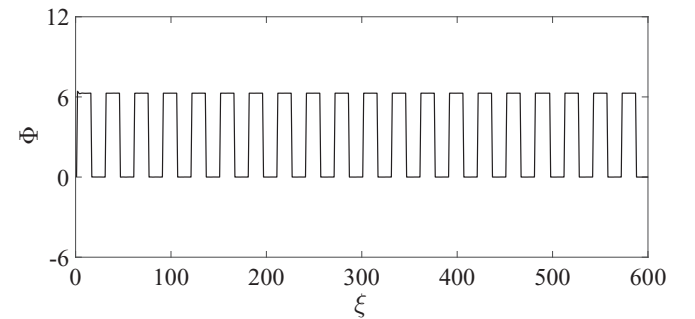


FIG. 5. Corresponding generalized phase of the soliton at the center of the transversal area vs the propagation distance when inputting the derived solution (25)–(29).

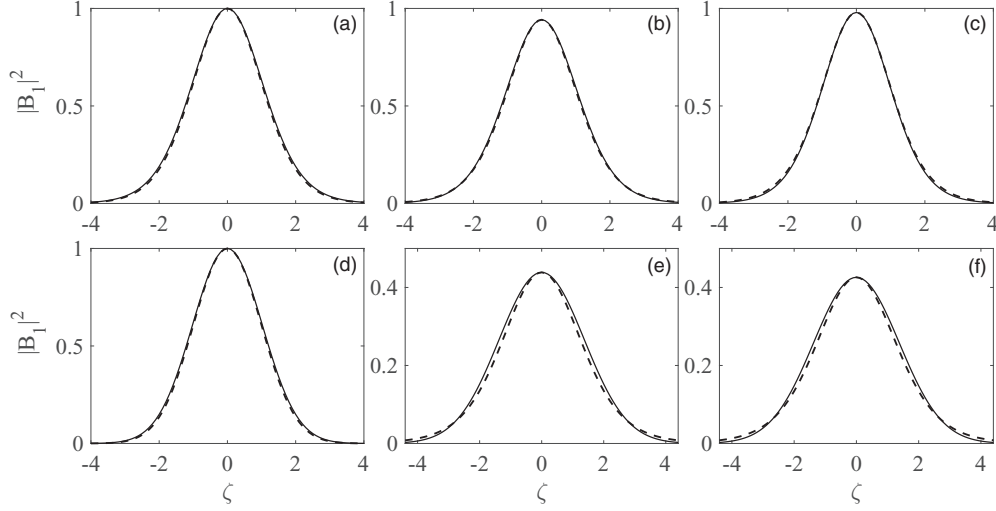


FIG. 6. Demonstration of changing space profiles during soliton propagation along longitudinal coordinates at $\xi = 0, 100, 200$ (first, second, and third columns, respectively) when inputting (a)–(c) the derived solution (25)–(29) and (d)–(f) the Gaussian ansatz (44) and (45). Solid lines are numerical results, and dashed lines are reference analytical profiles of the corresponding solutions.

domain was chosen as 204.8×204.8 dimensionless units or wider depending on the spreading of solitons. Transversal spectra of both harmonics amplitudes demonstrated the same qualitative behavior when we either expanded the integration domain or decreased the transversal step sizes. Supposing zero boundary conditions in space and time directions, we controlled their fulfillment in the process of computations. The difference scheme we applied has the property of the conservation of analogs of (41) and (42) at a lattice. The relative error usually was not greater than 10%. All the figures given below exploit the dimensionless quantities and are cut in transverse directions for better visualization.

Our numerical simulation is divided into three parts. In the first series of numerical experiments, we use the derived soliton solution (25)–(29) as a two-component input pulse. This case implies the phase- and group-velocity-matching conditions as well as the equality (3). We take the following ratios for the characteristic lengths provided that (27) and (30) hold:

$$l_D \approx 2.5 l_{nl}, \quad l_{dis} \approx 6.0 l_{nl}. \quad (43)$$

Numerical modeling confirms the stability of the derived solution (25)–(29) at both frequencies. Figure 2 shows the prop-

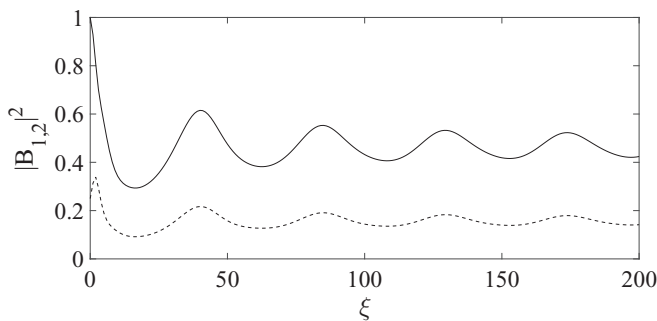


FIG. 7. Peak intensities of the fundamental (solid line) and second (dashed line) harmonics vs the propagation distance when inputting the Gaussian ansatz.

agation of spatial intensity profiles of the above-mentioned soliton solution at the fundamental frequency [Fig. 2(a)] and the doubled frequency [Fig. 2(b)] along the longitudinal coordinate ξ . The temporal profiles have similar intensity shapes. The simulation and observation were conducted up to $z = 600 l_{nl} = 240 l_D = 100 l_{dis}$. Figure 3 demonstrates the dependence of the peak intensities of both harmonics on the propagation coordinate ξ . We see that the regime of robust soliton propagation is established with the stabilization of energy exchange just for a few nonlinear lengths. This propagation is accompanied by the regular in-phase oscillations of peak intensities at both harmonics. At the same time, the oscillations

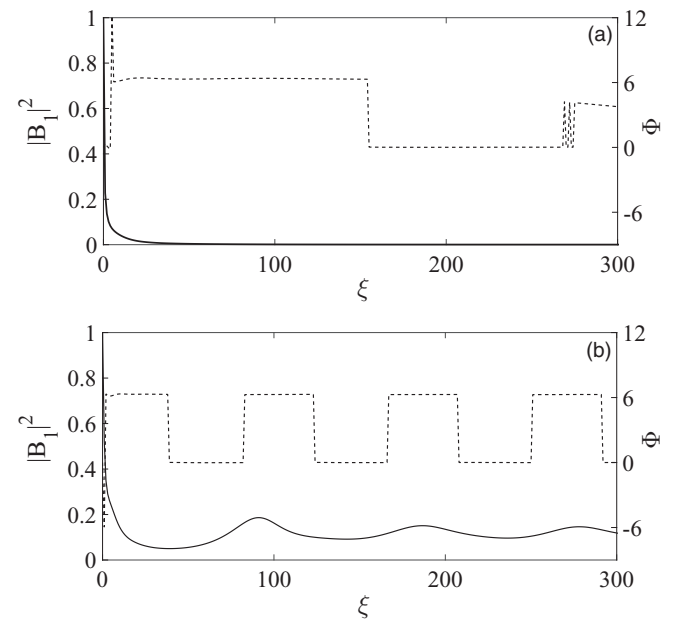


FIG. 8. Peak intensities of the fundamental harmonic (solid lines) and generalized phases (dashed lines) vs propagation distance for the following ratios of characteristic lengths: (a) $l_D^{\text{in}} = 0.05 l_{dis}$ and (b) $l_D^{\text{in}} = 0.12 l_{dis}$.

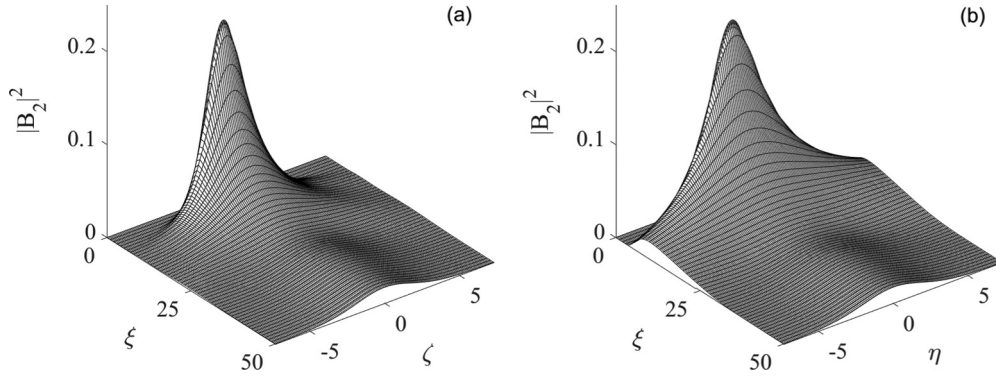


FIG. 9. Generation and dynamics of the second-harmonic pulse: (a) spatial intensity profile and (b) temporal intensity profile vs the propagation distance when inputting the pump pulse only.

of dimensionless spatial and temporal widths of the harmonics also have in-phase behavior, which is in-antiphase behavior for intensity oscillations (Fig. 4). This behavior defines the “breathing” character of soliton propagation. One should note that the observed absence of energy exchange between fundamental and second harmonics refers to the regime of classic parametric solitons. This regime is known as a reactive one, and an optimal relation between phases of interacting waves is a characteristic sign of it [22]. Figure 5 illustrates the dependence of the generalized phase $\Phi = 2\Phi_1 - \Phi_2$ on the distance ξ at the center of the (ζ, η) domain. The maxima of intensities and their corresponding minima of spatial and temporal widths coincide with the generalized phase jump down from 2π to 0. The minima of intensities and their corresponding maxima of spatial and temporal widths coincide with the generalized phase jump up from 0 to 2π . According to (40), the period of oscillations depends on both the diffraction length l_D and the dispersion length l_{dis} . Taking into account our selected ratios (43), we obtain the period of oscillations $T_s \approx 30l_{nl}$. We observe the same period in Figs. 3 and 4.

In connection with the results of the calculations presented above, it is interesting to simulate propagation of a pulse with the Gaussian initial profile. Recall that in [16] the authors investigated light bullets at quadratic nonlinearity, choosing the Gaussian ansatz as a trial one, and they numerically demonstrated a rather robust propagation of such bullets. We launch into a quadratic medium a bullet whose amplitude is

distributed as follows:

$$B_1 = \exp(-\zeta^2/4) \exp(-\eta^2/4), \quad (44)$$

$$B_2 = 0.5 \exp(-\zeta^2/4) \exp(-\eta^2/4). \quad (45)$$

In Figs. 6 and 7, we compare the obtained numerical results with the Gaussian ansatz (44) and (45). Reference analytical soliton profiles at distances presented in Fig. 6 were calculated as follows. The values of amplitudes and temporal and spatial half-widths were obtained from calculations and substituted in the analytical profiles. At first glance in both rows, we observe good agreement between numerical results and reference profiles. But comparing Figs. 3 and 7, we notice that the Gaussian ansatz yields mean dimensionless values of intensity at both harmonics that are twice as low. Upon varying the spatial and temporal widths of the Gaussian form bullet, we found a set of parameters providing stable propagation of a bullet with higher intensities. However, the search for such parameters is a rather tricky task. At the same time, the light bullet (25)–(29) is robust within a wide range of parameters determined by (39a).

The numerical simulations related to condition (39a) show that this condition is satisfied with quite good accuracy. For illustration purposes, in Figs. 8(a) and 8(b) the dynamics of peak intensity of the fundamental harmonic and the generalized phase are presented. We see that the pulse breaks up at $l_D^{in} = 0.05l_{dis}$ [Fig. 8(a)] and the corresponding dynamics of the generalized phase has irregular behavior. At

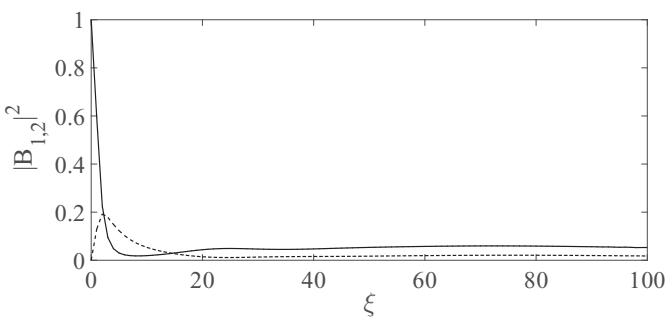


FIG. 10. Peak intensities of the fundamental (solid line) and second (dashed line) harmonics vs the propagation distance when inputting the pump pulse only.

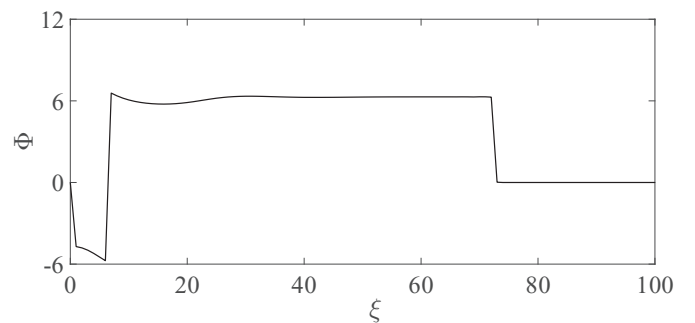


FIG. 11. Corresponding generalized phase of the soliton in the center of the transversal area vs the propagation distance when inputting the pump pulse only.

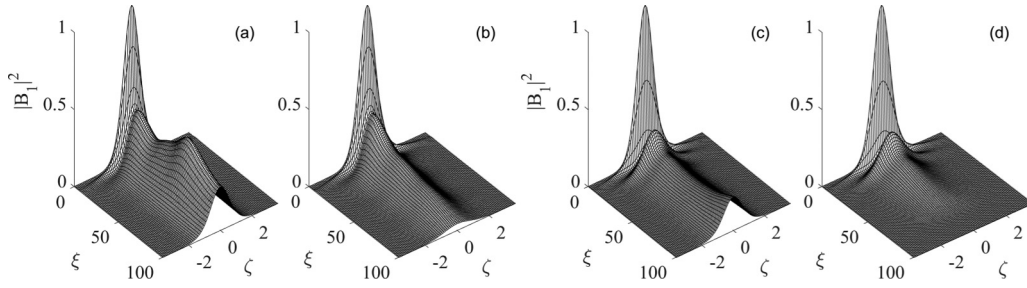


FIG. 12. Dynamics of the spatial intensity profile of the fundamental harmonic vs propagation distance at the edges of stability for the phase mismatch: (a) $\Delta q = 0.4$, (b) $\Delta q = 0.41$; and group-velocity mismatch: (c) $\sigma = 0.64$, (d) $\sigma = 0.65$.

the same time, under the condition $l_D^{\text{in}} = 0.12 l_{\text{dis}}$ [Fig. 8(b)] the dynamics of peak intensity and generalized phase have regular periodic behaviors. This corresponds to the formation of the spatiotemporal soliton.

The second series of numerical simulations is focused on the generation and formation of the two-component quadratic soliton. To organize the experiment, we launch a pulse in the form (25) only at the fundamental frequency. However, the ratios (43) do not lead to the formation of a soliton as both pulses quickly decay after second-harmonic generation. Nevertheless, we have managed to find the most favorable ratios in this case as

$$l_D \approx 2.5 l_{\text{nl}}, \quad l_{\text{dis}} \approx 6.7 l_{\text{nl}}. \quad (46)$$

Figure 9 depicts the propagation of the spatial intensity profile [Fig. 9(a)] and the temporal intensity profile [Fig. 9(b)] of the generated double-frequency wave along the longitudinal coordinate ξ . First, we observe the process of second-harmonic generation accompanied by diffractive [Fig. 9(a)] and dispersive [Fig. 9(b)] spreading. When the harmonics pass approximately $30 l_{\text{nl}}$, their spreading is compensated for by nonlinearity. Furthermore, a two-component bullet is formed and propagates with a solitonlike shape at both harmonics. Due to second-harmonic generation and energy losses caused by “tails,” the intensities of both harmonics are no more than 10% different from the value of the initial fundamental harmonic (Fig. 10). The spatial and temporal widths of the soliton increase in comparison to the initial values, and this is also a reason for the significant reduction in the intensities. Figure 11 shows the generalized phase dynamics along the coordinate ξ . It is worth noting that the optimal generalized phase is established after $30 l_{\text{nl}}$, corresponding to the bullet

regime shown in the first series of the numerical simulation. Because in (40) we considered only the first-order term in the expansion [see (35)], and we did not take into account the term of amplitude influence, we cannot use (40) here to estimate a period of oscillations.

In real experiments, we cannot neglect the influence of phase and group-velocity mismatches. It is well known that the effective generation of a second harmonic is possible provided there is complete phase-matching. In the majority of physical experiments, we deal with small phase mismatch or even with the cascading limit (large values of the phase mismatch). Therefore, we formulated the third series of computational experiments with the input solution (25)–(29) and small positive values of Δk and δ provided the ratios (43). As was expected, there are thresholds of Δk and δ after which the stable propagation of optical bullets breaks. In Fig. 12 the results corresponding to the close-to-threshold values of phase Δq ($\sigma = 0$) and group-velocity σ ($\Delta q = 0$) mismatches are presented. We observe that the formation of the bullet can take place if the values of Δq and σ lie in the range $0 \leq \Delta q \leq 0.4$ [Figs. 12(a) and 12(b)] and $0 \leq \sigma \leq 0.64$ [Figs. 12(c) and 12(d)]. At the first stage, propagation of pulses is also accompanied by the separation of “tails”. Consequently, the intensities at both frequencies become lower than in the case of phase and group-velocity matching. In numerical experiments with values beyond the thresholds ($\Delta q_{\text{cr}} = 0.4$, $\sigma_{\text{cr}} = 0.64$), both waves experience dispersion and diffraction broadenings, and solitons are not formed. In these cases, the last terms on the right-hand sides of Eqs. (1) and (2) are quickly oscillating on the z coordinate. Therefore, these terms can be neglected. Then (1) and (2) can be separated into two independent linear equations for A_1 and A_2 containing the dispersive and diffraction terms. It is clear that the pulse mode of the generation of second harmonics is impossible under such conditions. In Fig. 13 we summarize our findings on the mutual influence of phase and group-velocity mismatches on the stability of light bullet propagation.

V. CONCLUSION

Using the averaged Lagrangian method, we have obtained an analytical spatiotemporal solitary-wave solution to (2+1)D second-harmonic-generation equations. This solution has the form of a two-component planar light bullet. The “breathing” character is intrinsic to the bullet: its propagation along the longitudinal coordinate is accompanied by regular oscillations of intensities, temporal and transversal widths, etc. The

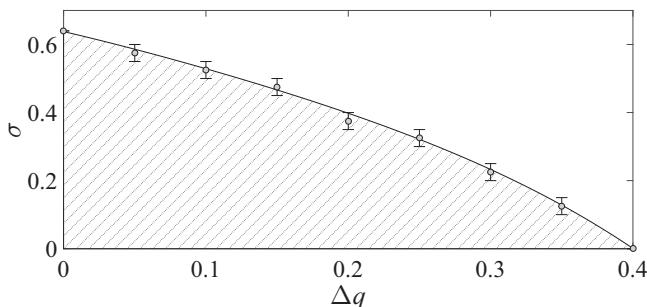


FIG. 13. Stability area (hatched) at the simultaneous presence of the phase and group-velocity mismatches.

condition of stability for the light bullet has been derived in an analytical form and verified numerically.

The correctness of the averaged Lagrangian method was confirmed by direct numerical simulation when we use the obtained analytical solution as the initial condition. There was good agreement between the analytical estimations and numerical results. In the process of numerical simulation, we demonstrated the formation of a weak two-component light bullet in the regime of second-harmonic generation. It is especially remarkable that the generated bullet replicates the form of the analytically derived solution. Low intensities at both frequencies are explained by the “tails” leaving the central part of the pattern, and by the increased widths.

The critical values of phase and group-velocity mismatches for soliton existence are obtained via numerical simulation. Below these values, light bullets are formed and propagate robustly. Above the thresholds, we observe the broadening of both pulses.

In summary, it seems feasible that the discussed spatiotemporal optical solitons will be observed experimentally. The experiment requires an anomalous dispersion at both frequencies. It can be achieved, for example, in a microdispersed (granulated) medium, where the manifestation of negative space dispersion depends on the ratio between the wavelength and the mean-square dimension of microinhomogeneities [29].

In the THz range, the frequencies ω and 2ω are below the frequencies of resonant absorption in such a medium. Therefore, the wave number for each frequency is $k \approx n_0\omega/c + \alpha\omega^3$, where under particular conditions α is a negative constant, and the cubic term is negligible in comparison with the linear one. In this case, we have an approximate fulfillment of the phase- and group-matching conditions. At the same time, $\beta_2 \equiv \partial^2 k / \partial \omega^2 = 6\alpha\omega$ and the relation for GVD coefficients (3) holds automatically. Then the formation of the above-mentioned light bullets becomes possible.

Let us assume that $\omega_0/\omega \sim 10-10^2$, $\tau_p \sim 100$ fs, and $\chi_0 \sim 10^{-2}$, where χ_0 is the linear susceptibility of the medium at $\omega = 0$. Using Sellmeier’s formula for χ_ω and taking into account that $2\pi\chi_0 \ll 1$ and $\omega^2/\omega_0^2 \ll 1$, we have $l_{nl} \sim l_{dis} \sim 1$ cm. This means that the distance $600l_{nl}$ in numerical simulations under these conditions corresponds to the order of 1–6 m. Assuming that granules are made of lithium niobate crystal (LiNbO₃), which has $\chi^{(2)} \sim 10^{-8}$ SGSE in the infrared range, we obtain the intensities $I_{1,2} \sim 10^6$ W/cm². Such relatively moderate intensities are available for various subpicosecond lasers in the infrared frequency range.

ACKNOWLEDGMENT

This work was supported by Russian Science Foundation (Project No. 17-11-01157).

-
- [1] R. McLeod, K. Wagner, and S. Blair, *Phys. Rev. A* **52**, 3254 (1995).
 - [2] G. D. McDonald, C. C. N. Kuhn, K. S. Hardman, S. Bennetts, P. J. Everitt, P. A. Altin, J. E. Debs, J. D. Close, and N. P. Robins, *Phys. Rev. Lett.* **113**, 013002 (2014).
 - [3] L. Bergé, *Phys. Rep.* **303**, 259 (1998).
 - [4] S. K. Turitsyn, *Theor. Math. Phys.* **64**, 797 (1985).
 - [5] D. E. Edmundson and R. H. Enns, *Opt. Lett.* **17**, 586 (1992).
 - [6] D. Mihalache, D. Mazilu, L.-C. Crasovan, I. Towers, A. V. Buryak, B. A. Malomed, L. Torner, J. P. Torres, and F. Lederer, *Phys. Rev. Lett.* **88**, 073902 (2002).
 - [7] G. Fibich and B. Ilan, *Opt. Lett.* **29**, 887 (2004).
 - [8] Y. V. Kartashov, B. A. Malomed, V. V. Konotop, V. E. Lobanov, and L. Torner, *Opt. Lett.* **40**, 1045 (2015).
 - [9] A. A. Kanashov and A. M. Rubenchik, *Physica D* **4**, 122 (1981).
 - [10] X. Liu, L. J. Qian, and F. W. Wise, *Phys. Rev. Lett.* **82**, 4631 (1999).
 - [11] X. Liu, K. Beckwitt, and F. Wise, *Phys. Rev. E* **62**, 1328 (2000).
 - [12] R. Šuminas, G. Tamošauskas, G. Valiulis, and A. Dubietis, *Opt. Lett.* **41**, 2097 (2016).
 - [13] H. Leblond, D. Kremer, and D. Mihalache, *Phys. Rev. A* **80**, 053812 (2009).
 - [14] D. Mihalache, D. Mazilu, L.-C. Crasovan, L. Torner, B. A. Malomed, and F. Lederer, *Phys. Rev. E* **62**, 7340 (2000).
 - [15] P. Y. P. Chen and B. A. Malomed, *Opt. Commun.* **282**, 3804 (2009).
 - [16] B. A. Malomed, P. Drummond, H. He, A. Berntson, D. Anderson, and M. Lisak, *Phys. Rev. E* **56**, 4725 (1997).
 - [17] D. V. Skryabin and W. J. Firth, *Phys. Rev. Lett.* **81**, 3379 (1998).
 - [18] C. R. Menyuk, R. Schiek, and L. Torner, *J. Opt. Soc. Am. B* **11**, 2434 (1994).
 - [19] J. A. Armstrong, *Phys. Rev. A* **11**, 963 (1975).
 - [20] S. V. Sazonov, *Phys. Wave Phenom.* **24**, 31 (2016).
 - [21] S. V. Sazonov, *J. Phys. Soc. Jpn.* **85**, 124404 (2016).
 - [22] Y. N. Karamzin and A. P. Sukhorukov, *Zh. Eksp. Teor. Fiz.* **20**, 734 (1974) [*JETP Lett.* **20**, 339 (1974)].
 - [23] S. K. Zhdanov and B. A. Trubnikov, *Zh. Eksp. Teor. Fiz.* **92**, 1612 (1987) [*Sov. Phys. JETP* **65**, 904 (1987)].
 - [24] S. K. Zhdanov and B. A. Trubnikov, *Quasi-gaseous Unstable Media* (Nauka, Moscow, 1991).
 - [25] E. A. Kuznetsov, A. V. Mikhailov, and I. A. Shimokhin, *Physica D* **87**, 201 (1995).
 - [26] S. A. Akhmanov, A. P. Sukhorukov, and R. V. Khokhlov, *Sov. Phys. Usp.* **10**, 609 (1968).
 - [27] P. Drummond, *Comput. Phys. Commun.* **29**, 211 (1983).
 - [28] B. Shizgal, *Spectral Methods in Chemistry and Physics* (Springer, The Netherlands, 2015).
 - [29] S. V. Sazonov, *Optika i Spektroskopiya* **79**, 282 (1995) [*Opt. Spectrosc.* **79**, 260 (1995)].